CHALMERS | UNIVERSITY OF GOTHENBURG

PREPRINT 2008:17

A Stokes model with cavitation for the numerical simulation of hydrodynamic lubrication

BERTIL NILSSON
PETER HANSBO

Department of Mathematical Sciences
Division of Mathematics
CHALMERS UNIVERSITY OF TECHNOLOGY
UNIVERSITY OF GOTHENBURG
Göteborg Sweden 2008

Preprint 2008:17

A Stokes model with cavitation for the numerical simulation of hydrodynamic lubrication

Bertil Nilsson, Peter Hansbo

Department of Mathematical Sciences
Division of Mathematics
Chalmers University of Technology and University of Gothenburg
SE-412 96 Göteborg, Sweden
Göteborg, April 2008

Preprint 2008:17
ISSN 1652-9715

Matematiska vetenskaper
Göteborg 2008

A Stokes model with cavitation for the numerical simulation of hydrodynamic lubrication

Bertil Nilsson [a], Peter Hansbo [b,*]

[a] *Center for Applied Mathematics and Physics, Halmstad University, SE-301 18 Halmstad, Sweden*

[b] *Department of Mathematics, Chalmers University of Technology, SE–412 96 Göteborg, Sweden*

Abstract

We present a cavitation model based on Stokes' equation and formulate adaptive finite element methods for its numerical solution. A posteriori error estimates and adaptive algorithms are derived, and numerical examples illustrating the theory are supplied, in particular with comparison to the simplified Reynolds model of lubrication.

Key words: cavitation, Stokes problem, adaptivity, error estimate

1 Introduction

The motivation for this work is the need for accurate computations of the hydrostatic pressure in a lubricant entrapped between the tool and workpiece in a metal forming process or in a sliding bearing. The ultimate goal is to be able to optimize the surface structure so as to maximize the lift from the pressure in the fluid. The usual tool for analyzing this problem is the Reynolds model [8], which however has severe limitations in that it is not well suited for handling large variations in the geometry of the lubrication layer. One way of decreasing resistance between the tool and workpiece is to make pits in the surface of the workpiece in order to generate cavitation with resulting pressure

* Corresponding author. Tel.: +46 31 772 1494.
Email address: peter.hansbo@chalmers.se (Peter Hansbo).

redistribution. If the pit geometry cannot be allowed to vary in an arbitrary fashion, optimization of the pit geometry becomes untenable.

In this paper, we will present a model for Stokesian flow with cavitation and formulate adaptive finite element methods for its solution. We will focus on control of the error in energy-like norms, and present numerical results comparing the Stokes model with the Reynolds model. We note that Reynolds model can be seen as a simplification of Stokes, cf. Bayada and Chambat [1], so it is to be expected that the range of applicability will be improved in a Stokes model (at the cost of computational complexity).

2 The continuous problem

Consider a domain Ω in $\mathbb{R}^n$, $n = 2$ or $n = 3$ with boundary $\partial\Omega$. We consider a lubricant with viscosity μ. The Stokes equation can then be written

$$-\mu\Delta\boldsymbol{u} + \nabla p = \boldsymbol{f} \text{ and } \nabla \cdot \boldsymbol{u} = 0 \quad \text{in } \Omega, \tag{1}$$

with, for ease of presentation, $\boldsymbol{u} = 0$ on $\partial\Omega$. Here, $\boldsymbol{u}$ is the velocity of the lubricant, p is the pressure, and $\boldsymbol{f}$ is a force term. The lubricant cannot support subatmospheric pressure, so an additional condition is $p \geq 0$ in Ω. In order to incorporate this condition into the model, it can be written as a variational inequality as follows. Let

$$K = \{p \in L_2(\Omega) : \quad p \geq 0\},$$

and seek $\boldsymbol{u} \in [H^1(\Omega)]^n$ and $p \in K$ such that

$$\int_\Omega \mu\nabla\boldsymbol{u} : \nabla\boldsymbol{v}\, d\Omega - \int_\Omega p\, \nabla \cdot \boldsymbol{v}\, d\Omega = \int_\Omega \boldsymbol{f} \cdot \boldsymbol{v}\, d\Omega, \quad \forall \boldsymbol{v} \in [H^1(\Omega)]^n \tag{2}$$

and

$$-\int_\Omega \nabla \cdot \boldsymbol{u}\,(q - p)\, d\Omega \leq 0, \quad \forall q \in K. \tag{3}$$

The well-posedness of this problem follows from the general theory presented by Brezzi, Hager, and Raviart [2].

3 Finite element approximation

3.1 Formulation

Let $\mathcal{T} = \{T\}$ be a locally quasiuniform triangulation of Ω into simplexes T of local mesh size h and let

$$V_h := \{\boldsymbol{v} \in [H_0^1(\Omega)]^n : \ \boldsymbol{v}|_T \in [P^2(T)]^n, \ \forall T \in \mathcal{T}\},$$

$$Q_h := \{q \in C^0(\Omega) : \ q|_T \in P^1(T), \ \forall T \in \mathcal{T}\},$$

i.e., we will use the well known Taylor-Hood element. We seek $(\boldsymbol{u}^h, p^h) \in V_h \times Q_h$ such that

$$\int_\Omega \mu \nabla \boldsymbol{u}^h : \nabla \boldsymbol{v} \, d\Omega - \int_\Omega p^h \, \nabla \cdot \boldsymbol{v} \, d\Omega = \int_\Omega \boldsymbol{f} \cdot \boldsymbol{v} \, d\Omega, \quad \forall \boldsymbol{v} \in V_h \tag{4}$$

and

$$-\int_\Omega \nabla \cdot \boldsymbol{u}^h \, (q - p^h) \, d\Omega \leq 0, \quad \forall q \in Q_h \cap K. \tag{5}$$

In order to solve the discrete system (4–5), we apply an iterative algorithm of Uzawa type [5]:

(1) Let $k = 0$ and choose an initial p_k^h.
(2) Solve the linear system (4) for the velocity field $\boldsymbol{u}_k^h$.
(3) Find the pressure corrector p_d from the system

$$\int_\Omega p_d q \, d\Omega = -\int_\Omega \nabla \cdot \boldsymbol{u}_k^h \, q \, d\Omega, \quad \forall q \in Q_h.$$

(4) Update the pressure field $p_{k+1}^h = P_\Lambda(p_k^h + p_d)$, where the operator $P_\Lambda(\vartheta) := \max(0, \vartheta)$.
(5) If the solution fails a given convergence criterion, set $k = k + 1$ and go back to step (2).

The projection P_Λ in (4) is applied pointwise on the nodal values for the pressure, which by construction leads to $p^h \in K$.

3.2 A posteriori *error control and adaptivity*

The question of error control for mixed variational inequalities has not been extensively treated in the literature. Though it fits in the general framework of Becker and Rannacher [9], the only paper the authors are aware of that explicitly treats the case at hand is [10], where, however, the fact that there

is a variational inequality not only for the multiplier, but also for the primal variable, is used in a crucial way. We shall here instead explore a simple alternative to [9,10] based on the observation that the cavitation problem is reminiscent of the Hencky problem in elasto–plasticity, and then follow Johnson and Hansbo [6] in deriving *a posteriori* error estimates. We then first consider the compressible case and consider the Stokes problem as the limit of the corresponding slightly compressible problem with the bulk modulus tending to infinity. The problem in question can be formulated as follows: Find the velocity $\boldsymbol{u}$ and the stress $\boldsymbol{\sigma}$ such that

$$\begin{aligned} \boldsymbol{\sigma} &= 2\mu\boldsymbol{\varepsilon}^D(\boldsymbol{u}) + \Pi(\kappa\nabla\cdot\boldsymbol{u})\ \mathbf{1} \quad \text{in } \Omega, \\ -\nabla\cdot\boldsymbol{\sigma} &= \boldsymbol{f} \quad \text{in } \Omega, \\ \boldsymbol{u} &= 0 \quad \text{on } \Gamma. \end{aligned} \tag{6}$$

Here, κ is the bulk modulus, $\mathbf{1}$ is the identity tensor, $\boldsymbol{\tau}^D = \boldsymbol{\tau} - \frac{1}{3}\ \mathrm{tr}\ \boldsymbol{\tau}\,\mathbf{1} = \boldsymbol{\tau} - \frac{1}{3}\ \left(\sum_{k=1}^3 \tau_{kk}\right)\mathbf{1}$ is the stress deviatoric corresponding to $\boldsymbol{\tau}$,

$$\boldsymbol{\varepsilon}(\boldsymbol{u}) = \frac{1}{2}\left(\nabla\otimes\boldsymbol{u} + (\nabla\otimes\boldsymbol{u})^{\mathrm{T}}\right)$$

is the symmetric part of the velocity gradient, and

$$\Pi(v) = \begin{cases} v \text{ if } v \le 0, \\ \\ 0 \text{ if } v > 0. \end{cases}$$

Finally, we use the notation

$$\nabla\cdot\boldsymbol{\sigma} = \left(\sum_{j=1}^n \frac{\partial\sigma_{ij}}{\partial x_j}\right)_{i=1}^n.$$

To simplify the analysis, we shall consider a regularized version of (6) in the form of a penalty method: Given $\gamma > 0$ small, find $(\boldsymbol{\sigma}_\gamma, \boldsymbol{u}_\gamma) \in H \times V$ such that

$$\begin{aligned} \frac{1}{2\mu}\boldsymbol{\sigma}_\gamma^D + \frac{1}{9\kappa}\mathrm{tr}\ \boldsymbol{\sigma}_\gamma\ \mathbf{1} + \frac{1}{\gamma}\left(\mathrm{tr}\ \boldsymbol{\sigma}_\gamma - \Pi(\mathrm{tr}\ \boldsymbol{\sigma}_\gamma)\right)\mathbf{1} &= \boldsymbol{\varepsilon}\left(\boldsymbol{u}_\gamma\right) \quad \text{in } \Omega, \\ \int_\Omega \boldsymbol{\sigma}_\gamma : \boldsymbol{\varepsilon}(\boldsymbol{v})\ d\boldsymbol{x} &= \int_\Omega \boldsymbol{f}\cdot\boldsymbol{v}\ d\boldsymbol{x} \quad \forall \boldsymbol{v} \in V, \end{aligned} \tag{7}$$

where (here we use $n = 3$ for simplicity)

$$V = \left[H_0^1(\Omega)\right]^3, H = \{\boldsymbol{\tau} = (\tau_{ij})_{i,j=1}^3 : \tau_{ij} = \tau_{ji} \in L_2(\Omega)\}.$$

Note that (7) formally tends to (6) as $\gamma \to 0$. The regularization is only introduced with the purpose of simplifying the statement and the proof of the *a posteriori* error estimate, and the actual value of the regularization parameter γ (small) will be insignificant. Introducing the notation

$$\boldsymbol{\eta}(\boldsymbol{\sigma}_\gamma) := \frac{1}{\gamma}\left(\text{tr } \boldsymbol{\sigma}_\gamma - \Pi(\text{tr } \boldsymbol{\sigma}_\gamma)\right)\mathbf{1},$$

we may write the problem on weak form as: find $\boldsymbol{\sigma} \in H$ and $\boldsymbol{u} \in V$ such that

$$\begin{aligned} a(\boldsymbol{\sigma}_\gamma, \boldsymbol{\tau}) + (\boldsymbol{\eta}(\boldsymbol{\sigma}_\gamma), \boldsymbol{\tau}) - (\boldsymbol{\varepsilon}(\boldsymbol{u}_\gamma), \boldsymbol{\tau}) = 0, \quad \forall \boldsymbol{\tau} \in H \\ (\boldsymbol{\sigma}_\gamma, \boldsymbol{\varepsilon}(\boldsymbol{u}_\gamma)) - (\boldsymbol{f}, \boldsymbol{v}) = 0, \quad \forall \boldsymbol{v} \in V. \end{aligned} \tag{8}$$

Here

$$(\boldsymbol{f}, \boldsymbol{v}) = \int_\Omega \boldsymbol{f} \cdot \boldsymbol{v}\, \mathrm{d}\boldsymbol{x}, \quad (\boldsymbol{\sigma}, \boldsymbol{\tau}) = \int_\Omega \boldsymbol{\sigma} : \boldsymbol{\tau}\, \mathrm{d}\boldsymbol{x},$$

and $a(\boldsymbol{\sigma}, \boldsymbol{\tau})$ is the *complementary energy* functional

$$a(\boldsymbol{\sigma}, \boldsymbol{\tau}) := \int_\Omega \left(\frac{1}{2\mu} \boldsymbol{\sigma}^D : \boldsymbol{\tau}^D + \frac{1}{3\kappa} \text{tr } \boldsymbol{\sigma}\, \text{tr } \boldsymbol{\tau} \right) d\Omega. \tag{9}$$

3.2.1 Error estimation in the complementary energy norm

We consider the following FEM formulation: find $(\boldsymbol{\sigma}_\gamma^h, \boldsymbol{u}_\gamma^h) \in H \times V_h$ such that

$$a\left(\boldsymbol{\sigma}_\gamma^h, \boldsymbol{\tau}\right) + \left(\boldsymbol{\eta}(\boldsymbol{\sigma}_\gamma^h), \boldsymbol{\tau}\right) = \left(\boldsymbol{\varepsilon}\left(\boldsymbol{u}_\gamma^h\right), \boldsymbol{\tau}\right) \tag{10}$$

for all $\boldsymbol{\tau} \in H$,

$$\left(\boldsymbol{\sigma}_\gamma^h, \boldsymbol{\varepsilon}\left(\boldsymbol{v}\right)\right) = (\boldsymbol{f}, \boldsymbol{v}) \tag{11}$$

for all $\boldsymbol{v} \in V_h$.

To obtain a first error estimate in complementary energy norm for the cavitation problem, we subtract the finite element problem from the continuous problem to obtain

$$a(\boldsymbol{\sigma} - \boldsymbol{\sigma}_\gamma^h, \boldsymbol{\tau}) + \left(\boldsymbol{\eta}(\boldsymbol{\sigma}_\gamma) - \boldsymbol{\eta}(\boldsymbol{\sigma}_\gamma^h), \boldsymbol{\tau}\right) = (\boldsymbol{\varepsilon}(\boldsymbol{u}) - \boldsymbol{\varepsilon}(\boldsymbol{u}_\gamma^h), \boldsymbol{\tau}) \quad \forall \boldsymbol{\tau} \in H.$$

We define $\|\boldsymbol{\sigma}\|_a^2 := a(\boldsymbol{\sigma}, \boldsymbol{\sigma})$ and $\boldsymbol{e}_u := \boldsymbol{u} - \boldsymbol{u}_\gamma^h$, and set $\boldsymbol{\tau} = \boldsymbol{\sigma} - \boldsymbol{\sigma}_\gamma^h$ to find that

$$\begin{aligned} \|\boldsymbol{\sigma} - \boldsymbol{\sigma}_\gamma^h\|_a^2 &= \left(\boldsymbol{\varepsilon}\left(\boldsymbol{u} - \boldsymbol{u}_\gamma^h\right), \boldsymbol{\sigma} - \boldsymbol{\sigma}_\gamma^h\right) - \left(\boldsymbol{\eta}(\boldsymbol{\sigma}_\gamma) - \boldsymbol{\eta}(\boldsymbol{\sigma}_\gamma^h), \boldsymbol{\sigma} - \boldsymbol{\sigma}_\gamma^h\right) \\ &\leq \left(\boldsymbol{\varepsilon}\left(\boldsymbol{e}_u\right), \boldsymbol{\sigma} - \boldsymbol{\sigma}_\gamma^h\right), \end{aligned}$$

where the last step follows from the following easily checked monotonicity relation:

$$(v - \Pi(v) - (w - \Pi(w)))\,(v - w) \geq 0.$$

Using the equilibrium equation, we note that

$$\left(\boldsymbol{\sigma} - \boldsymbol{\sigma}_\gamma^h, \boldsymbol{\varepsilon}\left(\boldsymbol{v}\right)\right) = 0 \quad \forall \boldsymbol{v} \in V_h,$$

so that

$$\|\boldsymbol{\sigma} - \boldsymbol{\sigma}_\gamma^h\|_a^2 \leq \left(\boldsymbol{\varepsilon}\left(\boldsymbol{e}_u - \pi_h \boldsymbol{e}_u\right), \boldsymbol{\sigma} - \boldsymbol{\sigma}_h\right),$$

where π_h denotes an interpolant or projection onto the mesh. Since

$$\boldsymbol{e}_u - \pi_h \boldsymbol{e}_u = \boldsymbol{u} - \boldsymbol{u}_\gamma^h - \pi_h \boldsymbol{u} + \pi_h \boldsymbol{u}_\gamma^h = \boldsymbol{u} - \pi_h \boldsymbol{u},$$

this can be written

$$\|\boldsymbol{\sigma} - \boldsymbol{\sigma}_\gamma^h\|_a^2 \leq \left(\boldsymbol{\varepsilon}\left(\boldsymbol{u} - \pi_h \boldsymbol{u}\right), \boldsymbol{\sigma} - \boldsymbol{\sigma}_h\right). \tag{12}$$

By integration by parts in (12) we find that

$$\begin{aligned} \|\boldsymbol{\sigma} - \boldsymbol{\sigma}_\gamma^h\|_a^2 \leq \sum_K \int_K \left(\boldsymbol{f} + \nabla \cdot \boldsymbol{\sigma}_\gamma^h\right) \cdot \left(\boldsymbol{u} - \pi_h \boldsymbol{u}\right) \, \mathrm{d}\boldsymbol{x} \\ -\frac{1}{2} \sum_K \int_{\partial K} \boldsymbol{n}_K \cdot [\boldsymbol{\sigma}_\gamma^h] \cdot \left(\boldsymbol{u} - \pi_h \boldsymbol{u}\right) \, ds, \end{aligned} \tag{13}$$

where $[\boldsymbol{\sigma}_\gamma^h]$ denotes the jump in stress between elements and $\boldsymbol{n}_K$ is the outward unit normal vector to the element. The estimate (13) can thus be used for the global error. To obtain an elementwise estimate to be used for mesh refinement purposes, we use Cauchy's inequality to obtain

$$\|\boldsymbol{\sigma} - \boldsymbol{\sigma}_\gamma^h\|_a^2 \leq \sum_K \omega_K \rho_K, \tag{14}$$

where, introducing the size h_K of element K,

$$\omega_K = \max \begin{cases} h_K^{-2} \|\boldsymbol{u} - \pi_h \boldsymbol{u}\|_{L_2(K)} \\ \\ h_K^{-3/2} \|\boldsymbol{u} - \pi_h \boldsymbol{u}\|_{L_2(\partial K)} \end{cases}$$

and

$$\rho_K = h_K^2 \|\boldsymbol{f} + \nabla \cdot \boldsymbol{\sigma}_\gamma^h\|_{L_2(K)} + \frac{1}{2} h_K^{3/2} \|\boldsymbol{n}_K \cdot [\boldsymbol{\sigma}_\gamma^h]\|_{L_2(\partial K)}.$$

We approximate the weights ω_K by

$$\omega_K \approx C_K^i \|D_h^2 \boldsymbol{u}_h\|_{L_2(K)}$$

where $C_K^i \approx 1$ is an interpolation constant, and where $D_h^2 \boldsymbol{u}_\gamma^h$ denotes a discrete approximation of the maximum second order derivative of $\boldsymbol{u}_\gamma^h$. The estimate (14) is not very sharp due to the fact that Cauchy's inequality has been used on each element. Thus it is better to use directly (13) when trying to assess the size of the error, and to use (14) as a refinement marker only.

Returning now to our original problem (4), we note that $p = -\lim_{\kappa\to\infty} \kappa\nabla\cdot\boldsymbol{u}$, and thus it is natural to interpret

$$\boldsymbol{\sigma}^h = \mu(\nabla \otimes \boldsymbol{u}^h)^{\mathrm{T}} - p^h\mathbf{1},$$

and use (14) with this stress. This is indeed what we have done in the following. We remark, however, that the *a posteriori* estimate can then only be formally correct if the space for the stresses is the same as that for the pressure, which is of course not the case for the Taylor-Hood element. To be strict, we would either need an element with $\nabla \cdot V_h \subset Q_h$ (which can only be achieved with nonconforming or stabilized methods) or use independent approximations for the stresses in the same space as the pressure. Thus, our *a posteriori* estimate can only serve as a roughly motivated guide for adaptivity for the kind of approximation we will use in the numerical examples below. We leave this point for future work.

For indication of which elements that are to be refined in the adaptivity process, the size of the element integrals in (14) is used as an indicator. We refine the 30% of the elements with the highest indicator in each adaptive step.

4 Numerical examples

In order to investigate the performance of the methods proposed, a few numerical examples will be presented. Unfortunately, experimental results demonstrating in detail the local behavior of the pressure and velocity images is, to our knowledge, not published. Though some integrated experimental results, such as lift, has been given by Etsion [3], [4] and Wang et. al. [11].

The object of our study is a single parabolic shaped oil pocket, see Figure 1. A central longitudinal cut through the gap between the metal sheet and work piece comprise our 2D computational model. The dimensions of the nominal channel and a particular pocket can be seen in Figure 2. Our aim is to study the behavior of the physics as the depth of the oil pocket increases while the opening width of the pocket and channel height stays the same. Boundary conditions used for the pressure is $p = 0$ at inlet and outlet. Velocity is set to zero along the floor of the channel and pocket boundary. The flow is driven by setting $u_x = 1, u_y = 0$ at the ceiling. The lubricant viscosity is $\mu = 1$.

The initial mesh has a typical element side length of 0.2. In Figure 2 we visualize the adaptive refinement progress yielding a sequence of meshes under consideration for a particular pocket depth. In each step the elements that give the largest third of the element contributions to the total error according to relation (14) are subdivided along their longest side into two new ones. After

refinement step 15 the area ratio is approximately 80 for the largest element to the smallest. Likewise, the longest element side over the shortest one is found to be about 20. The process gives a reasonable adaptivity taking place at the two sharp corners of the oil pocket, which of course are the two regions of the domain where a non-smooth solution can be expected.

The decrease of the total error according to refinement, measured by the number of nodes, is presented in Figure 3. Each dot indicates one adaptive step.

From a starting pressure $p = 0$ throughout the initial domain, the pressure field is passed on to the next refined mesh using linear interpolation during the adaptive process. Despite this, the typical number of iterations is 200, however decreasing with refinement level, for the Uzawa algorithm to converge according to $\|p_{k+1} - p_k\| < 10^{-9}$ for a particular mesh. All integrals involved are integrated using a 4-point Gauss quadrature scheme.

In Figure 4 we present, row wise for increased pocket depth, pressure and stream function contour lines. We can se from the stream lines that we have recirculation in the pocket for a pocket depth somewhere between row two and three. In the middle column the cavitation zone is identified as located at the sharp upstream edge of the pocket. An important point of this method is that we do not need to *a priori* define the boundary location between the fluid and cavitation phases. This is automatically taken care of by the refinement process.

A comparison of pressure at the ceiling between an adaptive Reynolds cavitation model, cf. [8], and the present Stokes cavitation model is given in Figure 5. The former presents a sharper pressure peak value, while the Stokes model shows a more smooth (and physically reasonable) variation. We remark that the classical way to approach the cavitation problem in the Reynolds community by first computing p^R from a pure Reynolds solution, followed by approximating $p \approx \max(0, p^R)$ (known as the half-Sommerfeld condition), is not very accurate compared to the cavitation models.

If we define impact to be the ratio of maximal channel height over minimal channel height Figure, 6 indicates that both models are capable of predicting an oil pocket impact of ≈ 1.7 as the best in terms of producing lift. This is in agreement with our earlier observation in Figure 4 indicating depth: we observe that as recirculation appears, lift is lost. A sequence of Figures 7-10 presents the mesh after 15 refinements and state of the flow for this particular pocket.

As the oil pocket depth increases the Reynolds model breaks down as can be seen in Figures 11-12. This is of course due to severe recirculation in the pocket, which does not conform with one of the basic assumptions (in our case, that of Couette flow) for the Reynolds model. However the Stokes model

remains stable.

5 Concluding remarks

We have presented an apparently novel approach to cavitation in Stokes flow, as an alternative to the cruder Reynolds model often used in lubrication analysis. We focus on the pressure drop as the source of cavitation, which has been criticized, e.g., by Joseph [7] as being dubious prom a physical point of view. However, unlike the Reynolds model, in which an *a priori* assumption is that the pressure drop is the source of cavitation, our approach has a wider range of applicability and can in principle make use of other cavitation models, such as those of [7]; it can also be used to model stretching of cavitation bubbles due to convective phenomena.

We have shown that our model yields results comparable to those of Reynolds in the range of flows for which the latter can be assumed to be valid, and that it is capable of predicting lift beyond the range of Reynolds model.

Future research will focus on cavitating flows for the full transient Navier–Stokes equations, for which a simple cavitation model such as ours can be an alternative for some aspects of cavitation, compared to more elaborate models incorporating several physical phenomena.

References

[1] G. Bayada, M. Chambat, The transition between the Stokes equation and the Reynolds equation: a mathematical proof, Appl. Math. Optim. 14 (1986) 73–93.

[2] F. Brezzi, W.W. Hager, P.-A. Raviart, Error estimates for the finite element solution of variational inequalities. Part II. Mixed methods, Numer. Math. 31 (1978) 1–16.

[3] I. Etsion, L. Burstein, A model for mechanical seals with regular microsurface structure. Tribology Transactions 39 (1996) 677–683.

[4] I. Etsion, Y. Kligerman, G. Halperin, Analytical and Experimental Investigation of Laser-Textured Mechanical Seal Faces, Tribology Transactions 42 (1999) 511–516.

[5] R. Glowinski, Numerical Methods for Nonlinear Variational Problems, Springer-Verlag, New York, 1984

[6] C. Johnson, P. Hansbo, Adaptive finite element methods in computational mechanics, Comput. Methods Appl. Mech. Engrg. 101 (1992) 143–181.

[7] D. D. Joseph, Cavitation and the state of stress in a flowing liquid, J. Fluid Mech. 366 (1998) 367–378.

[8] B. Nilsson, P. Hansbo, Adaptive finite element methods for hydrodynamic lubrication with cavitation, Int. J. Numer. Methods Engrg. 72 (2007) 1584–1604.

[9] R. Becker, R. Rannacher, An optimal control approach to a posteriori error estimation in finite element methods, Acta Numer. 10 (2001) 1–102.

[10] F.-T. Suttmeier, On computational methods for variational inequalities, Comput. Mech. 35 (2005) 401–408.

[11] X. Wang, K. Kato, A. Adachi, K. Aizawa, Load carrying capacity map for the surface texture design of SiC thrust bearing sliding in water, Tribology International 36 (2003) 189–197.

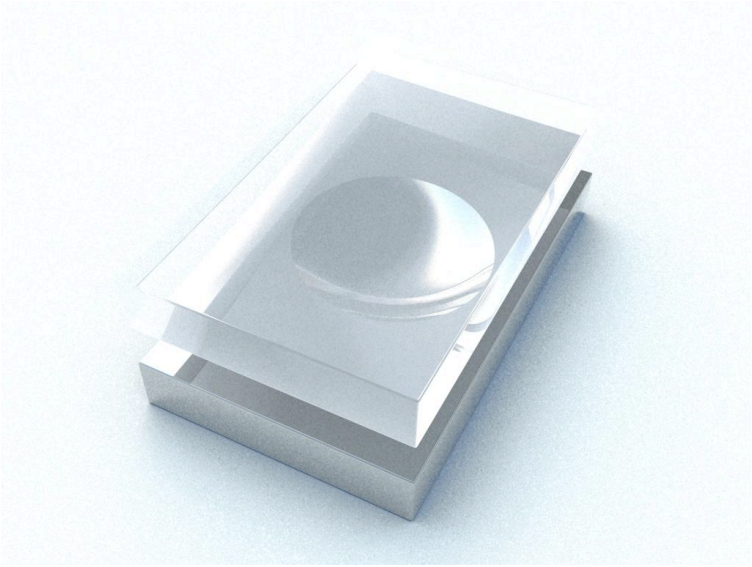

Fig. 1. Oil pocket model.

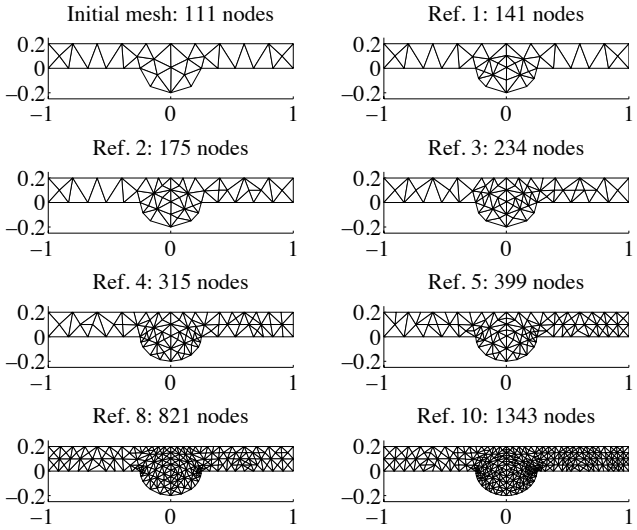

Fig. 2. Sequence of refined meshes.

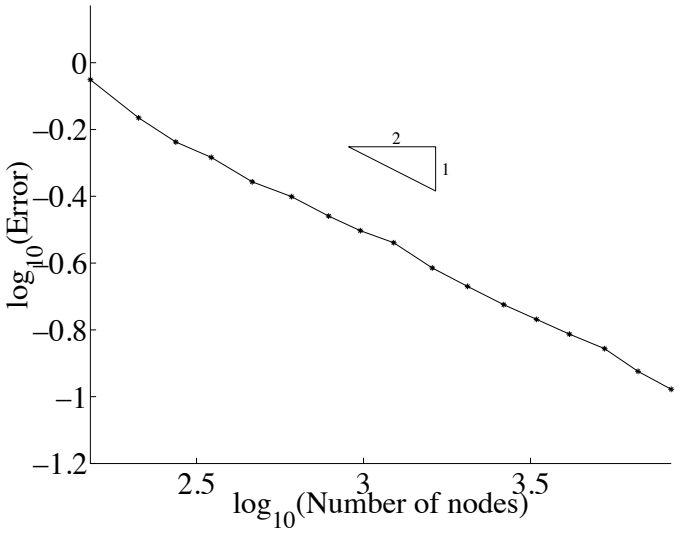

Fig. 3. Convergence for right hand side of error estimation (14).

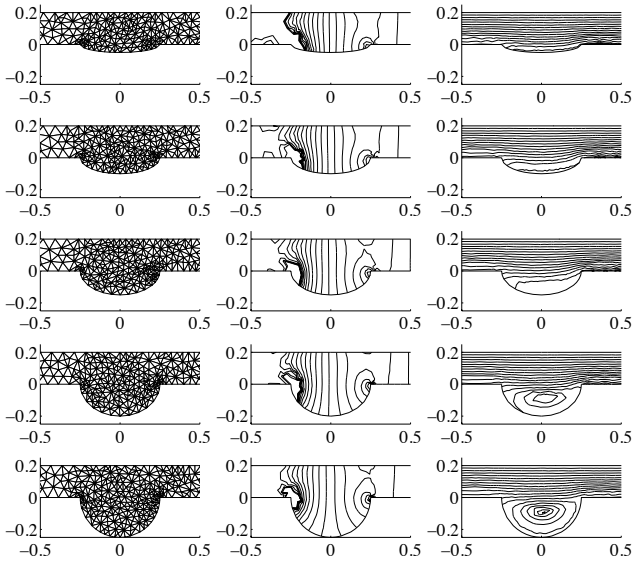

Fig. 4. Mesh, pressure and stream function contour lines for increasing depth of the oil pocket.

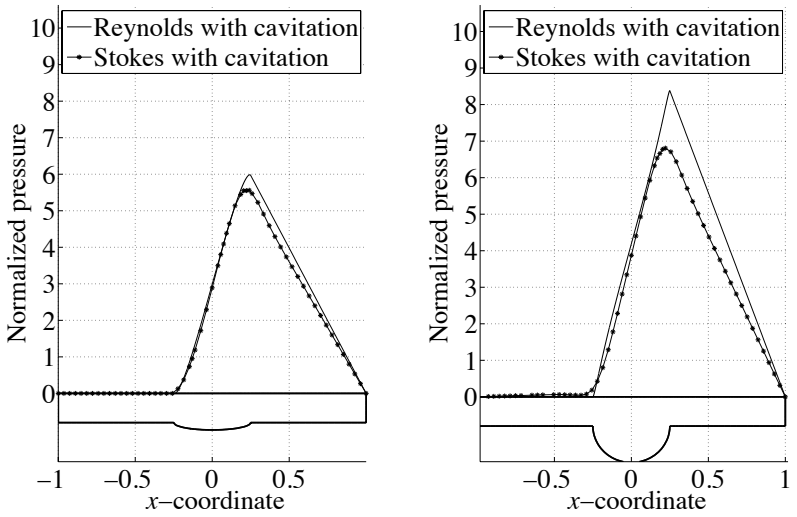

Fig. 5. Pressure at the ceiling for Reynolds and Stokes cavitation models for a shallow pocket and a rather deep one.

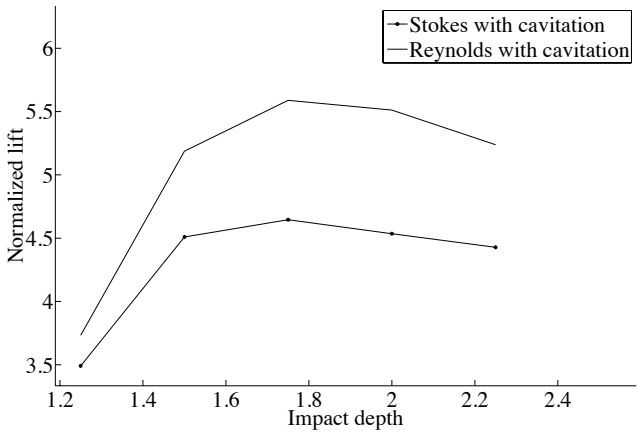

Fig. 6. Lift for Stokes and Reynolds according to impact of the oil pocket.

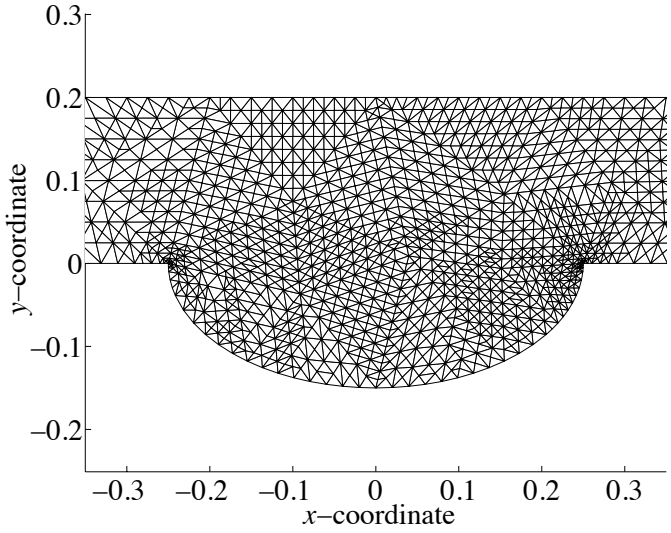

Fig. 7. Element mesh zoom.

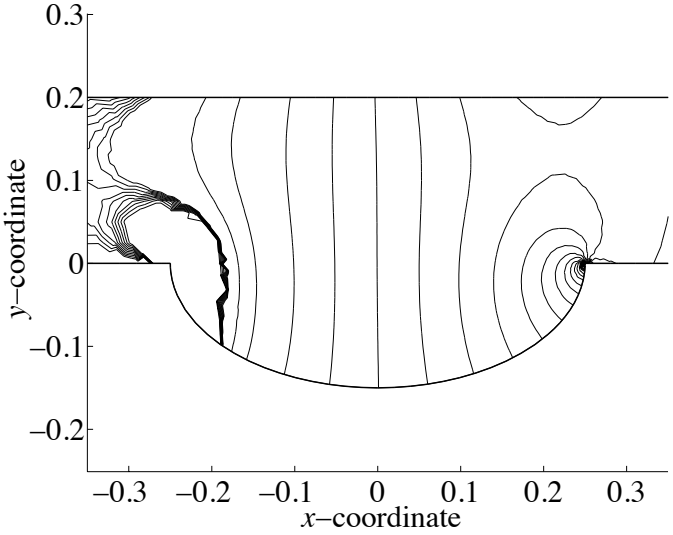

Fig. 8. Pressure contour lines.

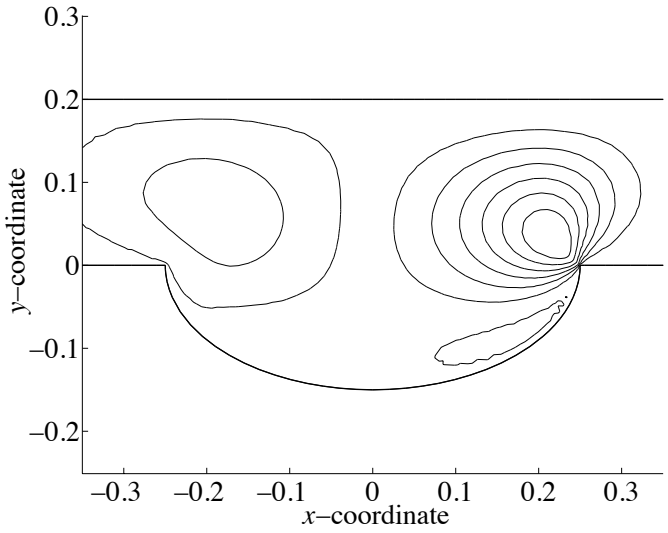

Fig. 9. Velocity u_y contour lines.

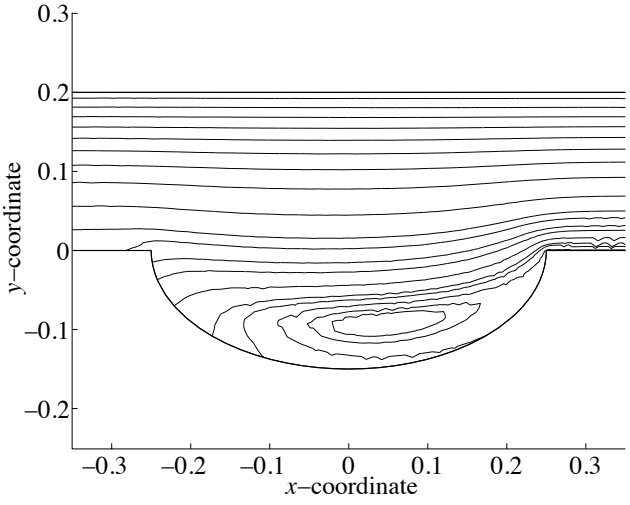

Fig. 10. Stream function contour lines.

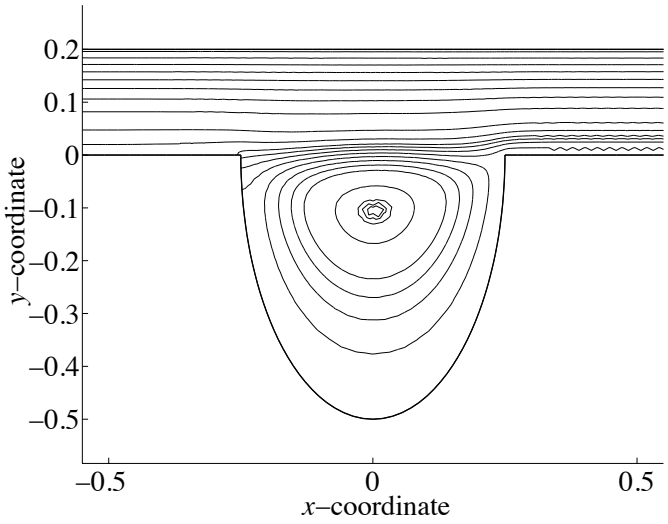

Fig. 11. Stream function contour lines for a very deep pocket.

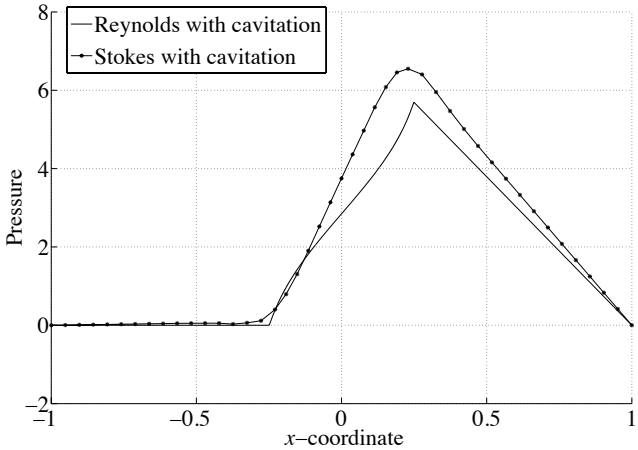

Fig. 12. Pressure at ceiling for Reynolds and Stokes for a very deep pocket.